



# Anticorrosion Effect of Silicon Nitride and Zirconium Diboride Composite on Ni–P–Zn Electroless Deposition on Mild Steel

O. Kilanko<sup>1</sup> · O. S. I. Fayomi<sup>1,2</sup> · A. A. Sode<sup>1</sup>

Received: 1 May 2020 / Revised: 9 June 2020 / Accepted: 1 July 2020 / Published online: 8 July 2020  
© Springer Nature Switzerland AG 2020

## Abstract

Electroless nicked-based deposition on mild steel surface from a nickel–zinc phosphate bath with  $\text{NiSO}_4 \cdot 6\text{H}_2\text{O}$ ,  $\text{ZnSO}_4 \cdot 7\text{H}_2\text{O}$ , and  $\text{NaH}_2\text{PO}_2 \cdot \text{H}_2\text{O}$  salt in the presence of silicon nitrides and zirconium diboride as additives at a constant time was studied. The structural evolution of electroless deposited mild steel surface was characterized for crystal change formation using a scanning electron microscope (SEM) and elemental quantification done using energy-dispersive spectroscopy (EDS). The electrochemical corrosion analysis of the deposited mild steel with and without composite additives was analyzed using linear polarization resistance and open circuit potential in both  $\text{H}_2\text{SO}_4$  and  $\text{NaCl}$  solution. From the results, significant presence and the effect of wt% of additives were noticeable on the electroless mild steel surface. Ni–P–Zn in the presence of  $10\text{ZrBr}_2$  and  $10\text{Si}_3\text{N}_4$  actively provide an induced weight gain of 0.0974 g and 0.0973 g, respectively. A correspondent,  $0.034 \text{ g/m}^2$  coating per unit area of zirconium diboride additives, was obtained against  $0.030 \text{ g/m}^2$  for silicon nitrides. The structural evolution shows proper homogeneous crystal formation and stable packed additive concentrated at the lattices with EDS showing the presence of induced peak. From the corrosion assessment result, electroless deposited mild steel with Ni–P–Zn– $10\text{ZrBr}_2$  and Ni–P–Zn– $10\text{Si}_3\text{N}_4$  with optimum particle concentration shows better corrosion resistance performance with a corrosion rate of 0.5048 mm/year, and 5.1347 mm/year, as against the unadditive deposition with 11.393 mm/year in  $\text{NaCl}$  solution.

**Keywords** Electroless · Anticorrosion · Coating · Mild steel

## 1 Introduction

Corrosion exit globally on a global scale with leading nations possessing the best technological advancements and resources in material sciences still incurring costs [1]. Corrosion appears in various forms with metal and non-metal due to ionic activities and molecular species [2]. The detrimental effect of corrosion failure on metal's lifespan, structures, tools, and equipment is akin to natural calamities such as floods, hurricanes, fires, tornadoes, and others [3]. In real-life applications, metals are of utmost importance, and

the most popular metal is no stranger to gradual degradation due to corrosion mechanisms [4].

Mild steel is a form of steel, with about 0.15–0.45% of carbon [5]. It possesses excellent mechanical properties to structural, chemical, and construction responses. Mild steel offers unique toughness characteristics and durability, especially for automotive parts, chemical processing plants, and manufacturing sectors were excellent formability and fabrication prospects are required [6]. Although mild steel has proven to possess versatility in significant industries because of its ease to acquire, recycle tendency, and moderate cost in purchase yet it has low corrosion resistance properties in the face of ionic species resulting in severe corrosion failures and fatigues [7].

Several preventive efforts such as surface coating, materials selection, inhibitor, cathodic protection, and design route have been employed to combat the widespread corrosion devastation and mechanism [8]. Coating technology has been seen as a functional route capable of withstanding extreme harsh conditions posed by erosion, wear, friction, temperature gradient, and corrosion. It is a mature

✉ O. S. I. Fayomi  
ojo.fayomi@covenantuniversity.edu.ng;  
Ojosundayfayomi3@gmail.com

<sup>1</sup> Department of Mechanical Engineering, Covenant University, P.M.B 1023, Ota, Nigeria

<sup>2</sup> Department of Chemical, Metallurgical and Materials Engineering, Tshwane University of Technology, P.M.B. X680, Pretoria, South Africa

convectonal technology that significantly improves performance structural orientation and distribution of ultra-fine crystal [9]. Composite provides a thin film layer in defense of the underlay surface either for decorative purposes and functional applications. Coating industries where the useful composite is used are unlimited, among which are power generation for turbine blade, household devices, printing industries, and chemical pipelines, etc. [10].

Deposition through electroless bath solution is a unique route to obtain thin layer films on the prepared surface through autocatalytic activities of the aqueous bath constituent with no galvanic presence [11]. Compounds of the metallic ions provide a reducing effect through cation electrons over the substrate [12]. The nickel-based electroless coating has been known to give crystallized fused nickel plating as a protective layer on the steel [13]. Electroless nickel coating can also possess multifunctional properties through metal-ion induced system for pitting corrosion prevention [14].

With a lot of development of recent with electroless nickel metal coating, challenges have been seen with the choice of composite additive and their suitability in bath framework [15–18]. Particulate additives in composite form provide exceptional functional performance and regulate the process parameter until better coating efficiency is attained [19–22]. Research has shown that the use of composite particulate often influences coating characteristics by reducing bath stress initiation, enhances bath flow, serves a brightener, and reduces cracks pores [22–25]. Although the application of composite nickel-based is still revolving, there is a need to find a suitable stable composite material to support the challenge posed by nickel–phosphate coating in controlling the bath framework for proper coating performance [26–30].

Electroless nickel phosphate coating is considered with challenges arising from coating structural instability, adhesion, and pitting corrosion on a metallic surface, hence the significant need to further improve the usage for technological and service purposes [31–33]. This study aims to establish the effect of functional composite properties of silicon nitrides and zirconium diboride on nickel-phosphate electroless deposition on mild steel at constant time and weight concentration with target for marine pipe union.

**Table 2** Additive particulate composition in electroless bath

Particulate additives	Volumetric ratio in g/L
Si <sub>3</sub> N <sub>4</sub>	5
Si <sub>3</sub> N <sub>4</sub>	10
ZrBr <sub>2</sub>	5
ZrBr <sub>2</sub>	10

## 2 Experimental Methods

### 2.1 Sample Preparation

The mild steel plate used in the study was sectioned into a rectangular shape of 40 mm × 40 mm × 2 mm with the help of struers discotom precision cutter at 600 rpm. The steel plate purchased from a metal processing vendor in Ota, Nigeria, was analyzed accordingly. The percentage nominal weight composition of the mild steel substrate is presented in Table 1. The corrosion propagation was done using AUTO LAB PGSTAT 101 potentiostat galvanostat device with Nova 2.1 software. The structural properties of the starting materials were analyzed using SEM/EDS. All chemical reagents used are Analar grade and conformed to standard for electroless setup. The bath formulation was prepared a day to the deposition proper for even dispersion in line with study by [5].

### 2.2 Electroless Bath and Formulation

All chemical used in this study was obtained and supplied to Surface Engineering Research Laboratory, Covenant University from Sigma-Aldrich, USA. NiSO<sub>4</sub>·6H<sub>2</sub>O, ZnSO<sub>4</sub>·7H<sub>2</sub>O, and NaH<sub>2</sub>PO<sub>2</sub>·H<sub>2</sub>O salt were obtained in powder nature. NiSO<sub>4</sub>·6H<sub>2</sub>O, which is the based salt, has a density of 2.07 g/cm<sup>3</sup>, solubility in water of 77.5 g/mL at 30 °C. ZrBr<sub>2</sub> is characterized by its hexagonal refractory structure with a tendency to withstand high temperatures. It has a density of 6.08 g/cm<sup>3</sup>. The Si<sub>3</sub>N<sub>4</sub> composite is thermodynamics stable with a density of 3.17 g/cm<sup>3</sup>. The weight percentage of the ZrBr<sub>2</sub> and Si<sub>3</sub>N<sub>4</sub> was selected over 5–10 g after several optimizations. The bath formulation was obtained by dissolving in 1 L of deionized water 30 g of NiSO<sub>4</sub>·6H<sub>2</sub>O, 5 g of ZnSO<sub>4</sub>·7H<sub>2</sub>O, 33 g of NaH<sub>2</sub>PO<sub>2</sub>·H<sub>2</sub>O, 60 g of C<sub>6</sub>H<sub>5</sub>·Na<sub>3</sub>O<sub>7</sub>·2H<sub>2</sub>O, 25 g of (NH<sub>4</sub>)<sub>2</sub>SO<sub>4</sub>, 10 g of H<sub>3</sub>BO<sub>3</sub>, 10 g of Thiourea at pH of 5. The bath was allowed to dissolve appropriately after leaving it for 24 h. Most of the admixtures constituting the bath formulation are for quick conductivity of cation, brightener, buffers, and

**Table 1** Compositional value in weight% of mild steel substrate

Element	S	Mn	Si	Ni	Al	P	C	Fe
Composition (%)	0.02	0.15	0.016	0.01	0.01	0.01	0.032	Balance

refiners. Table 2 present the additives particulate composition for the electroless deposition.

### 2.3 Electroless Set-Up

No direct current was used in this study since the process involves autocatalytic activities. The bath is put into a non-reactive container with 500 mL, a conical flask made from glass, and placed on a hot stirrer. The contents of the bath are heated to a temperature range of  $85 \pm 50$  °C with the help of a metal bulb thermometer. The mild steel samples were suspended by a simple beam structure into the heated compound, and given sufficient time to develop a thin film layer. Each sequential coating deposition was done for an uninterrupted time of 50 min at a stirring rate of 250 rpm to ensure uniformity of coating. The components of the bath were changed after each time cycle with the addition of the particles  $ZrB_2$  and  $Si_3N_4$ , at concentrations of 5 g/L and 10 g/L. After each experimental process, according to deign in Table 3, the samples were air-dried and stored in a cool and dry place.

### 2.4 Analysis of Electroless Deposited Samples

The structural characteristics of the developed electroless nickel–phosphate and nickel–phosphate-induced composite additive were examined using a scanning electron microscope (SEM) and energy-dispersive spectroscopy (EDS). The VEGA 3, TESCAN model SEM function by examining surface morphology, crystal orientation, grain deposit, and particle inclusion with the coating lattices.

### 2.5 Corrosion Analysis

The spontaneous chemical interaction of the electroless deposited mild steel coating was examined using the potentiodynamic polarization technique. The produced coating samples were subjected to acidic and sea likes (salty) environments at an ambient temperature of  $(27 \pm 1)$  °C). A three conventional electrode cell consisting of the reference electrode, working electrode, and counter electrode with a

beaker filled with 100 mL of electrolyte was used. With the mild steel as the working electrode, silver chloride as the reference electrode, and graphite rod as the counter electrode, the configuration was connected to AUTO LAB PGSTAT 101 Metrohm. The Tafel plot was attained within  $- 1.5$  V and  $+ 1.5$  V and a scan rate of 0.0012 V/s at several concentrations and while changing the temperature of the system.

$$IE(\%) = \frac{(J_{corr})_a - (J_{corr})_p}{(J_{corr})_a} * 100 \tag{1}$$

where,  $(I_{corr})_a$  and  $(I_{corr})_p$  represent the corrosion density ( $A/cm^2$ ) in the absence and presence of the particulate, respectively.

The corrosion rate (CR) is determined using the equation below:

$$CR(mm/year) = \frac{0.00327 * J_{CORR} * E_w}{D} \tag{2}$$

where  $J_{CORR}$  is the current density in  $\mu A/cm^2$ ,  $D$  is the density of copper  $g/cm^3$  ( $8.96 g/cm^3$ ),  $E_w$  is the equivalent weight in gram of mild steel.

## 3 Results and Discussion

### 3.1 Electroless Deposition Results

The effect of constant time and particle variation on weight gain and coating per unit area is presented in Tables 3 and 4, respectively. The particulate  $Si_3N_4$  and  $ZrB_2$  additions on Ni–P–Zn electroless bath deposited on mild steel substrate at 50 min, and particulate concentration of (0 g, 5 g, and 10 g) provide a deposit gain. The impacts of the submicron crystal were seen to promote weight addition noticed in Table 3. The weight gain of Ni–P–Zn– $ZrB_2$  and Ni–P–Zn– $Si_3N_4$  composite coating were generally better with 10 $ZrB_2$  possessing 0.0974 g and 10 $Si_3N_4$  having 0.0973, respectively. The result attains with no composite additive has the lowest with a corresponding value of 0.0250 g.

**Table 3** Effect of constant time and particle concentration on weight gain of electroless Ni–P–Zn series

Sample label	Deposition time (minutes)	Weight gain (grams)
Ni–P–Zn	50	0.0250
Ni–P–Zn–10 $Si_3N_4$	50	0.0973
Ni–P–Zn–05 $Si_3N_4$	50	0.0437
Ni–P–Zn–10 $ZrBr_2$	50	0.0974
Ni–P–Zn–05 $ZrBr_2$	50	0.0440

**Table 4** Effect of constant time and particle concentration on coating thickness of electroless Ni–P–Zn series

Sample label	Deposition time (minutes)	Coating per unit area ( $g/m^2$ )
Ni–P–Zn	50	0.010100
Ni–P–Zn–10 $Si_3N_4$	50	0.030406
Ni–P–Zn–05 $Si_3N_4$	50	0.013656
Ni–P–Zn–10 $ZrBr_2$	50	0.034688
Ni–P–Zn–05 $ZrBr_2$	50	0.022250

From Table 4, the position of all composite addition in Ni–P–Zn formation also follows the same trend demonstrated in Table 3 with Ni–P–Zn–ZrB<sub>2</sub> at maximum having 0.034688 A/m<sup>2</sup> and 0.0030406 A/m<sup>2</sup> for Ni–P–Zn–Si<sub>3</sub>N<sub>4</sub>. It implies that particles of the second phase affect the thin film content of the electroless coated Ni–P–Zn matrix. A similar observation has been notified by the reported literature [14–17].

### 3.2 Structural Evolution Studies of Unplated and Electroless Plated Samples

The surface crystal morphology of the unplated and electroless-deposited nickel phosphate zinc coating on mild steel with and without composite additives are analyzed using a scanning electron microscopy supported by energy-dispersive spectroscopy. Figure 1 shows the SEM image of the unplated mild steel surface. The starting micrograph of composite particles of Si<sub>3</sub>N<sub>4</sub> and ZrB<sub>2</sub> are presented in Figs. 2 and 3, respectively. Figure 4 shows the SEM/EDS image of Ni–P–Zn without additives at ×500 magnification. With an uninterrupted time of 50 min, the micrograph reveals the dispersion of grey-like nature with spot analysis revealing its richness in nickel phosphate zinc deposit. The dominant composition of Ni, Zn, and P constituent show by the EDS is expected due to bath formation. Thus, there is a thin film formation within the mild steel substrate. However, close observation of the structure in Fig. 4 shows there is open-pore evolution in form of porosity, which is often seen with ordinary nickel-based electroless deposition as a result of the autocatalysis process parameter.

The effect of composite additive on the micrograph is seen at the mild steel surface for Si<sub>3</sub>N<sub>4</sub> particle, as presented

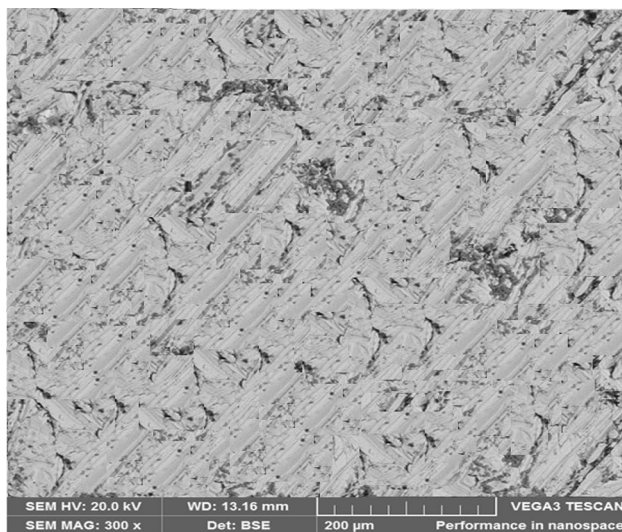


Fig. 1 SEM result of mild steel surface

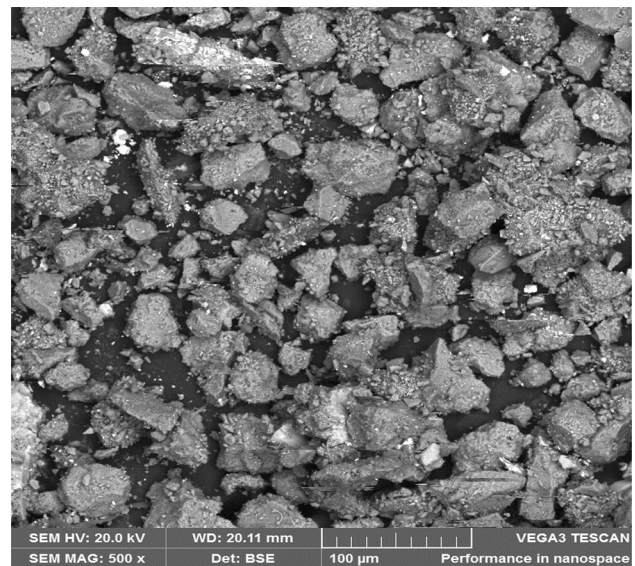


Fig. 2 SEM characterization of Si<sub>3</sub>N<sub>4</sub> composite

in Fig. 5. The observation shows that the electroless-coated surface uniformly protected by Si<sub>3</sub>N<sub>4</sub> particle integrated into the Ni–P–Zn matrix. It is good to mention that though, there was coating stability, and proper adhesion, the effect of particulate size evolution on the surface was noticed with few clustering of Si<sub>3</sub>N<sub>4</sub> surrounded at Ni lattice in form of agglomeration. Interestingly, the microstructural features are free from surface defect but generally bright and closely packed grain providing sufficient protection and grain refinements. Consistence look with the study by [32, 33] shows that second phase composite like Si<sub>3</sub>N<sub>4</sub> is often posed into

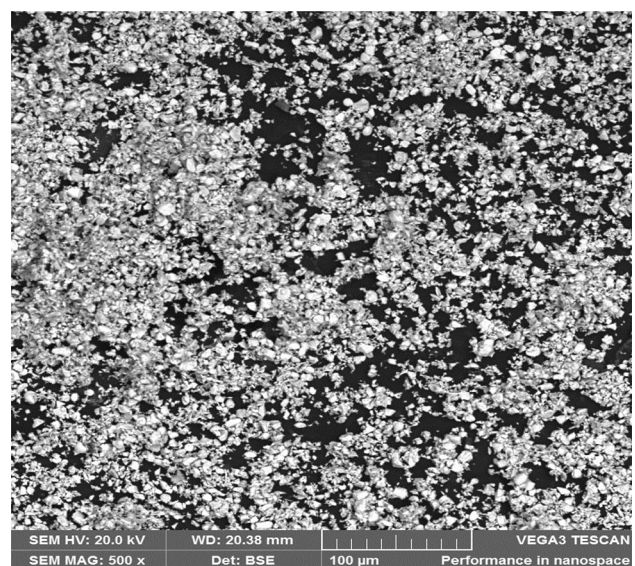
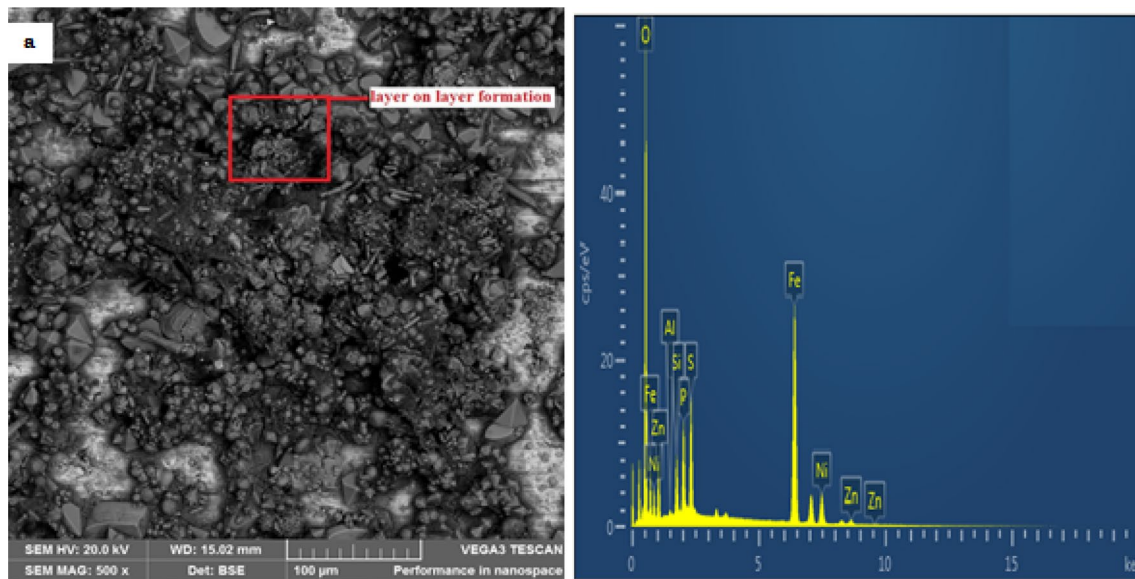
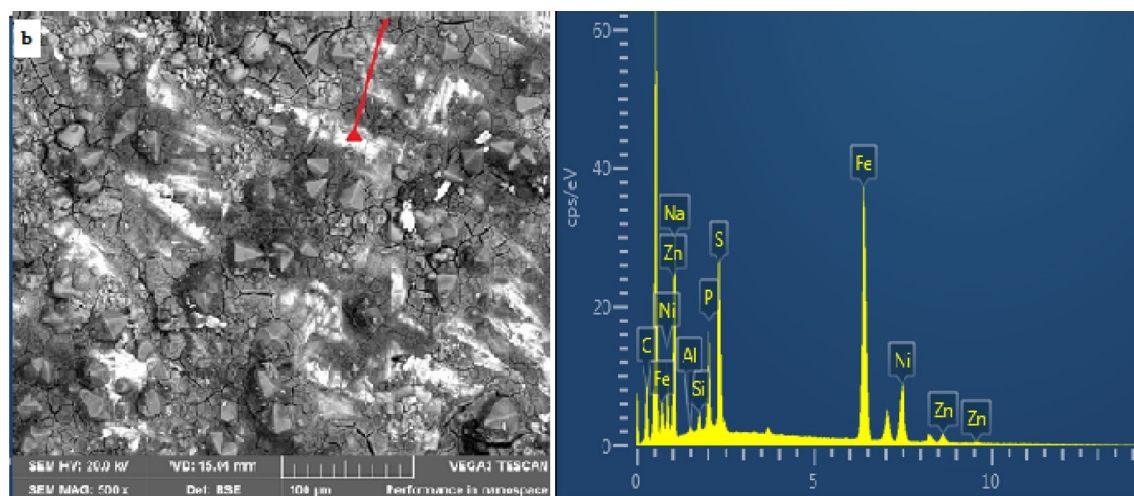


Fig. 3 SEM characterization of ZrB<sub>2</sub> composite



**Fig. 4** SEM/EDS result of Ni–P–Zn particulate on mild steel surface at  $\times 500$  magnification



**Fig. 5** SEM/EDS result of Ni–P–Zn– $\text{Si}_3\text{N}_4$  particulate on mild steel surface at  $\times 500$  magnification

the Ni–P pores like nodular protrusions through diffusive chemistry phenomena. Moreover, deposition process parameters, especially with a higher time gradient, also assist in the formative crystal stability induced into the vacancies. EDS studies also affirmed the quantification of a major diffused elements with Ni, Si, and Zn forming stable nodular bounds.

The SEM/EDS of the Ni–P–Zn– $\text{ZrB}_2$  is showed in Fig. 6 with a change in the structural evolution and dispersed homogeneously distributed particulate within the Ni interstitials. The difference in the predominately distributed particle in a smaller size can be due to active composite chemistry and its influence on the process parameter

[1]. Although, one could notice that instead of the composite particle to exhibit a flake-like nature, it possesses a completely diffused propagation causing perfect metal-electrolyte mode of robust crystal growth, which are rare. With the orientation of Ni– $\text{ZrB}_2$  with less 10 g of a particle, a proper peak was not seen, unlike structure noticed in Fig. 5 of the same amount of particle incorporation. Thus, this could be due to the charge of  $\text{Ni}^{2+}$  ion forming a solid sheath on  $\text{ZrB}_2$ . A similar justification could be that since the process involve autocatalysis rather than electrophoresis, a prevailing model by might be supported where particle adsorbed on the substrate and considerably grows into the metal matrix through particle charged and

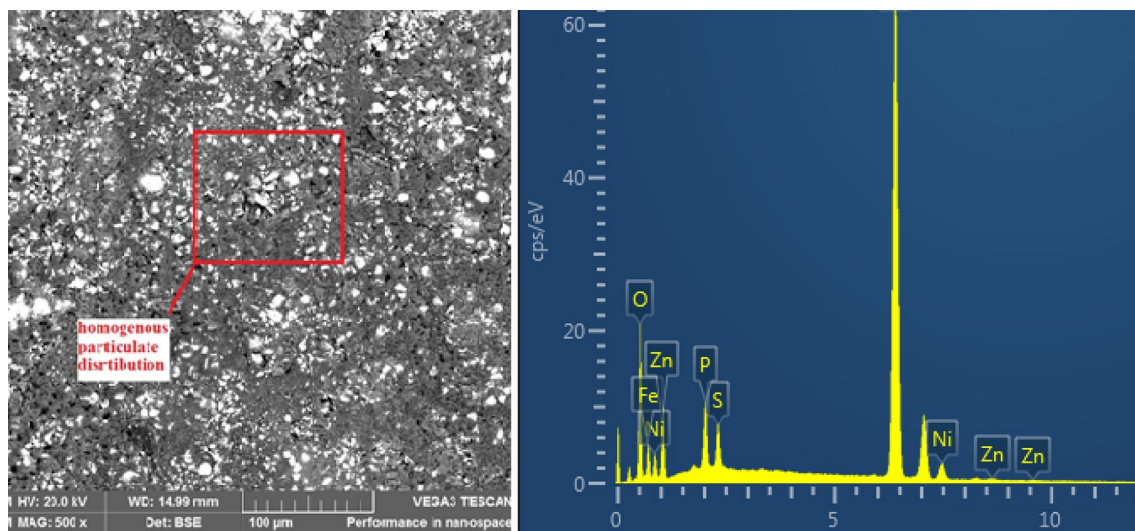


**Fig. 6** SEM/EDS result of Ni-P-Zn-ZrBr<sub>2</sub> particulate on mild steel surface at ×500 Magnification

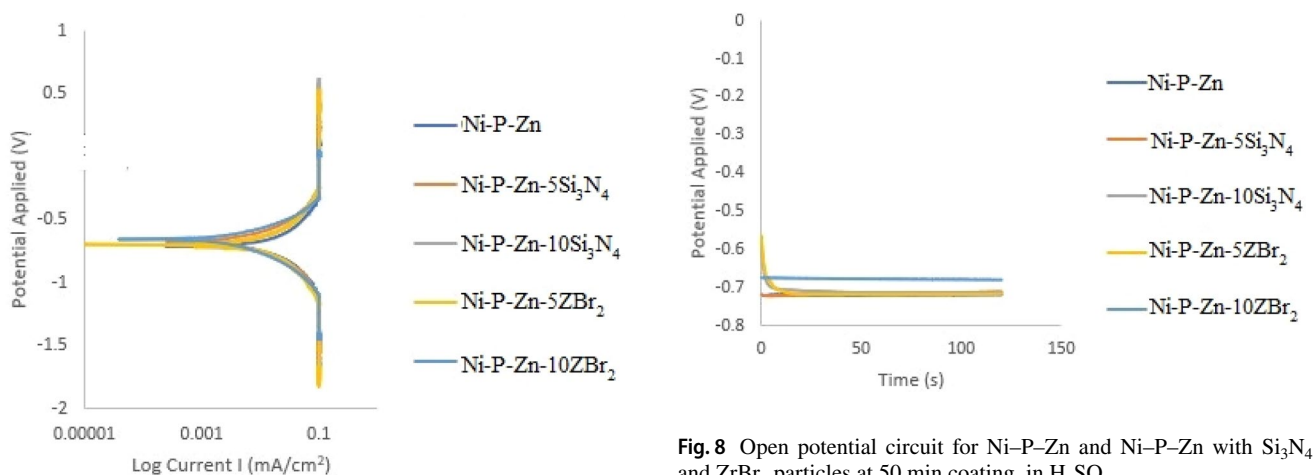


**Fig. 7** Potentiodynamic polarization plot for Ni-P-Zn and Ni-P-Zn with Si<sub>3</sub>N<sub>4</sub> and ZrBr<sub>2</sub> particles at 50 min coating, in H<sub>2</sub>SO<sub>4</sub>

high-temperature gradient leading to homogenous refinement and new morphology.

### 3.3 Corrosion Analysis of Electroless Deposited Composite on Mild Steel

The corrosion integrity and vulnerability of the deposited electroless Ni-P-Zn and composite-induced matrix with Si<sub>3</sub>N<sub>4</sub> and ZrBr<sub>2</sub> were shown in Figs. 7, 8, 9 and 10 through potentiodynamic polarization plots and open circuit potential. The coatings were examined in simulated 3.65 wt% of sodium chloride (NaCl) and 0.5 M tetraoxosulphate (VI) acid (H<sub>2</sub>SO<sub>4</sub>). Figure 7 shows potentiodynamic polarization plot for Ni-P-Zn and Ni-P-Zn with Si<sub>3</sub>N<sub>4</sub> and ZrBr<sub>2</sub>

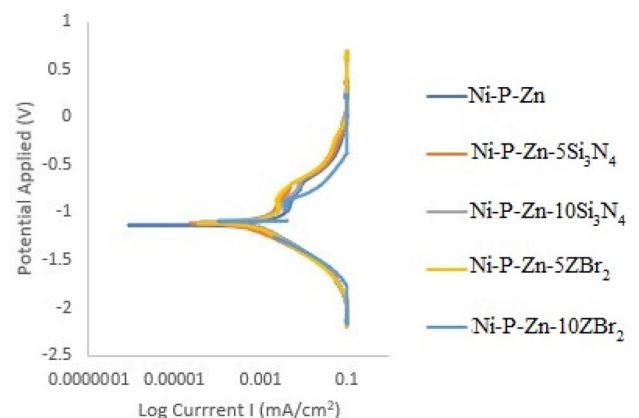


**Fig. 9** Potentiodynamic polarization plot for Ni-P-Zn and Ni-P-Zn with Si<sub>3</sub>N<sub>4</sub> and ZrBr<sub>2</sub> particles at 50 min coating, in NaCl

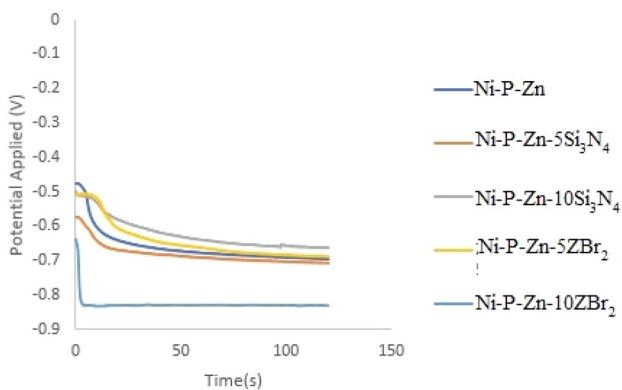


**Fig. 10** Open circuit potential plot for Ni-P-Zn and Ni-P-Zn with Si<sub>3</sub>N<sub>4</sub> and ZrBr<sub>2</sub> particles at 50 min coating, in NaCl

particles at 50 min coating, in H<sub>2</sub>SO<sub>4</sub>. Figure 8 shows an open potential circuit for Ni-P-Zn and Ni-P-Zn with Si<sub>3</sub>N<sub>4</sub> and ZrBr<sub>2</sub> particles at 50 min coating, in H<sub>2</sub>SO<sub>4</sub>. Figure 9 shows the potentiodynamic polarization plot for Ni-P-Zn and Ni-P-Zn with Si<sub>3</sub>N<sub>4</sub> and ZrBr<sub>2</sub> particles at 50 min coating, in NaCl. Figure 10 shows an open circuit potential plot for Ni-P-Zn and Ni-P-Zn with Si<sub>3</sub>N<sub>4</sub> and ZrBr<sub>2</sub> particles at 50 min coating, in NaCl. The Tafel data extrapolated from the Tafel plot in acid and chloride solution are shown in Tables 5 and 6, respectively.

From Fig. 7 the cathodic and anodic branch obtained for all developed alloy are quite similar an evident of the same corrosion activities. A substantial degradation trend was observed from the Tafel data in Table 5. The corrosion rate from the extrapolated data shows that electroless Ni-P-Zn coating has (13.569 mm/year), which is almost twice higher of the best composite induced electroless coating with (7.2238 mm/year). A corresponding corrosion current density of 0.00011677 A/cm<sup>2</sup> against Ni-P-Zn-ZrBr<sub>2</sub> with 0.00062167 A/cm<sup>2</sup> was also established. By observing the CR, R<sub>p</sub>, J<sub>corr</sub>, and E<sub>corr</sub>, it can be affirmed that there is an

**Table 5** Potentiodynamic polarization figures for Ni-P-Zn and particulate deposition at 50 min coating, in H<sub>2</sub>SO<sub>4</sub>

Sample label	E <sub>corr</sub> (V)	J <sub>corr</sub> (A/cm <sup>2</sup> )	Corrosion rate (mm/year)	Polarization resistance (Ω)
Ni-P-Zn	- 0.65258	0.0011677	13.569	4.7801
Ni-P-Zn-10Si <sub>3</sub> N <sub>4</sub>	- 0.69329	0.0006811	7.9143	13.677
Ni-P-Zn-05Si <sub>3</sub> N <sub>4</sub>	- 0.67058	0.0006216	8.7702	6.1702
Ni-P-Zn-10ZrBr <sub>2</sub>	- 0.70722	0.0006216	7.2238	14.847
Ni-P-Zn-05ZrBr <sub>2</sub>	- 0.69079	0.0007300	8.4834	12.053

**Table 6** Potentiodynamic polarization figures for Ni-P-Zn and particulate deposition at 50 min coating, in NaCl

Sample label	E <sub>corr</sub> (V)	J <sub>corr</sub> (A/cm <sup>2</sup> )	Corrosion rate (mm/year)	Polarization resistance (Ω)
Ni-P-Zn	- 1.1010	0.00098051	11.393	49.100
Ni-P-Zn-10Si <sub>3</sub> N <sub>4</sub>	- 1.1346	0.00022650	2.6319	83.909
Ni-P-Zn-05Si <sub>3</sub> N <sub>4</sub>	- 1.1099	0.00048664	5.6470	54.432
Ni-P-Zn-10ZrBr <sub>2</sub>	- 1.1734	0.00004340	0.5048	112.28
Ni-P-Zn-05ZrBr <sub>2</sub>	- 1.1169	0.00044165	5.1319	55.772

improved and stable corrosion resistance trend for all deposited composite induced electrolyte. However, an established study by [6, 8] has noted that induced composite particulate can always retard pitting corrosion evolution due to solid crystal packed interface from the structural build-up of the coated surface [23–25]. Also observed that H<sub>2</sub> evolution and sulfide halides provide an insignificant effect in most metal matrix composite coating due to the presence of second phase particle participation in the Ni lattice. This effect is also seen with the open circuit potentials curve presented in Fig. 8 with composite developed alloy leading performance.

It must be noted that the polarization resistance R<sub>p</sub> and corrosion rate C<sub>R</sub> obtained from sodium chloride-induced environment on the electroless plated coating reveals that there is much change in the corrosion behavior of the Ni-P-Zn-ZrBr<sub>2</sub> matrix as against the Ni-P-Zn coating. Though Ni-P-Zn-ZrBr<sub>2</sub> matrix has the best performance among all developed composite phases, it possesses geometric polarization resistance R<sub>p</sub> of 112.28 (Ω), Corrosion rate C<sub>R</sub> of 0.5048 mm/year. The best in the Ni-P-Zn-10Si<sub>3</sub>N<sub>4</sub> series also has great resistance to corrosion susceptibility with R<sub>p</sub> of 83.909 (Ω), Corrosion rate C<sub>R</sub> of 2.6319 mm/year. The coating without additives of both Si<sub>3</sub>N<sub>4</sub> and ZrBr<sub>2</sub> has a higher corrosion rate and lower polarization resistance influence with R<sub>p</sub> of 49.100 (Ω), Corrosion rate C<sub>R</sub> of 11.393 mm/year. It can be seen that the change in deposition causes a significant difference in the electrochemical performance of the developed electroless coated mild steel even in the presence of Cl<sup>-</sup> ion. Thus, the composite particles impact maximally as a protective barrier against corrosion vulnerability. This significant dispersive behavior as substantial refinement is due to the individual composite constituent [16].

After the electrochemistry study, the corroded surfaces at the best performance were subjected to OPM analysis to locate pit and corrosion products within the deposit. Figure 11 shows the morphology of corroded Ni-P-Zn

particulate on mild steel surface at  $\times 10$  magnification in NaCl. The surface interface was seen with full-blown corrosion products across the lattice identified to be pre-occupied by nickel phosphate zinc coating. This shows that the stability of the coating over a more extended period could not be ascertained in the presence of chloride ions solution. Figures 12 and 13 show a better improved and consistent surface retardation against chloride penetration due to the presence of  $\text{Si}_3\text{N}_4$  and  $\text{ZrBr}_2$  hybrid with nodular shape grains still present in large quantities at the interface. This considerable significant improvement is a result of the crystal compartment that is stable within the operating parameter of the developed electroless composite coating.

#### 4 Conclusion

Ni–P–Zn– $\text{ZrBr}_2$  and Ni–P–Zn– $\text{Si}_3\text{N}_4$  coating were developed through the autocatalytic route containing sub-micron composite particle on a mild steel plate. From microstructural study, a new crystal orientation was seen due to incorporated particles. Thus, homogeneous interface with less agglomeration was attained. The nodular crystal packed structure was achieved with a higher concentration of particle, providing finer and stable coating about the weight gain. With the corrosion properties, the outcome of the potentiodynamic polarization and open circuit potential shows that deposited electroless composite coating possesses a higher corrosion resistance effect with

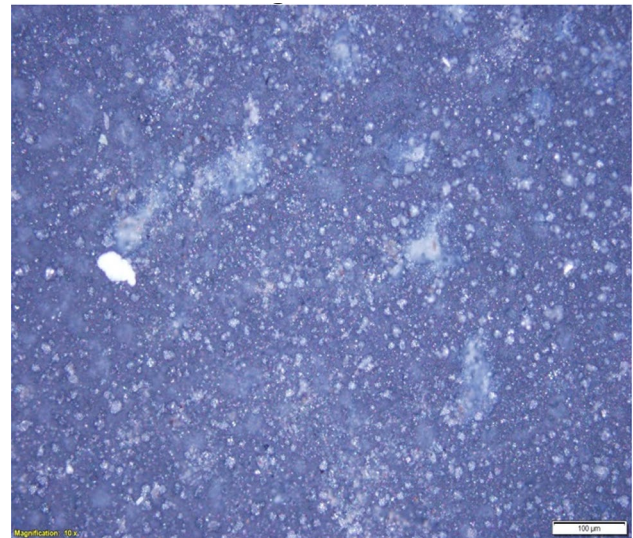


**Fig. 12** Optical morphology of corroded Ni–P–Zn– $\text{Si}_3\text{N}_4$  particulate on mild steel surface at  $\times 10$  magnification

lower corrosion current density when compared to coating with Ni–P–Zn. It is worth mentioning that the corrosion resistance of mild steel reduces drastically with the presence of an incorporated particle. From the pitting effect, the corrosion evolution reduces drastically especially with composite-induced coatings.

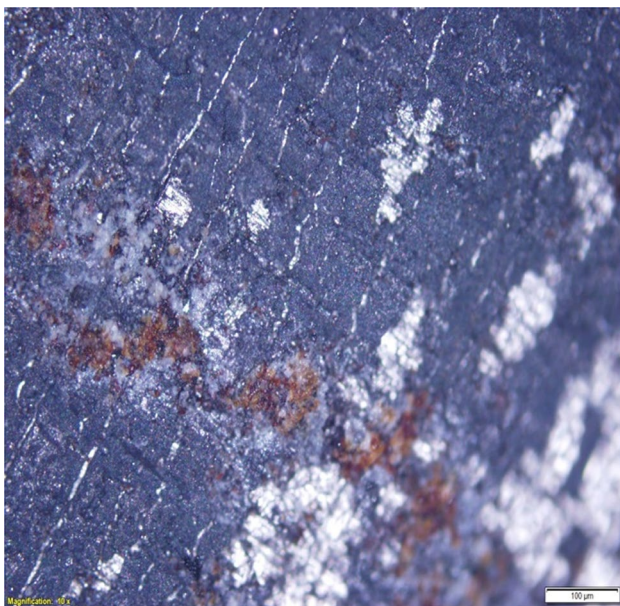


**Fig. 11** Optical morphology of corroded Ni–P–Zn particulate on mild steel surface at  $\times 10$  magnification

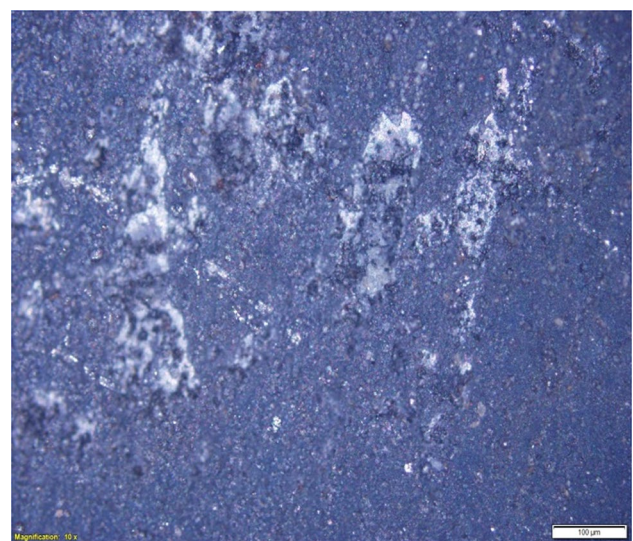


**Fig. 13** Optical morphology of corroded Ni–P–Zn– $\text{ZrBr}_2$  particulate on mild steel surface at  $\times 10$  magnification



**Acknowledgements** The authors appreciate gracefully the financial support of Covenant University and Surface Engineering Research Laboratory, Department of Mechanical Engineering, Covenant University for equipment usage.

## Compliance with Ethical Standards

**Conflict of interest** The authors will like to declare that this research has no any financial or work related competing interest.

## References

- Balaraju JN, Radhakrishnan PV, Ezhilselvi A, Kumar AA, Chen Z, Surendran KP (2016) Studies on electroless nickel polyalloy coatings over carbon fibers/CFRP composites. *Surf Coat Technol* 302:389–397
- Koch GH, Brongers MP, Thompson NG, Virmani YP, Payer JH (2002) Corrosion cost and preventive strategies in the United States. US Federal Highway Administration, Washington, DC. <https://www.nace.org/uploadedFiles/Publications/ccsupp.pdf>
- Anawe PAL, Fayomi OSI, Popoola API (2017) Results in physics investigation of microstructural and physical characteristics of nano composite tin oxide-doped  $Al^{3+}$  in  $Zn^{2+}$  based composite coating by DAECD technique. *Results Phys* 7:777–788
- Ashby MF (2011) Engineering materials 1: an introduction to properties, applications and design. *Mater Sel Mech Des* 1:1–464
- Aydođdu GH, Aydinol MK (2006) Determination of susceptibility to intergranular corrosion and electrochemical reactivation behaviour of AISI 316L type stainless steel. *Corr Sci* 48(11):3565–3583
- Ayoola AA, Fayomi OSI, Ogunkanmbi SO (2018) Data in brief data on inhibitive performance of chloraphenicol drug on A315 mild steel in acidic medium. *Data Brief* 19:804–809
- Akinyemi OO, Nwaokocho CN, Adesanya AO (2012) Evaluation of corrosion cost of crude oil processing industry. *J Eng Sci Technol* 7(4):517–518
- Amin MM, Kee LK, Yunus K (2002) The process of electroplating in the presence of nickel salts. *Ultra Sci* 14(3):309–318
- Dai J, Liu X, Zhai H, Liu Z, Tian J (2009) Preparation of Ni-coated  $Si_3N_4$  powders via electroless plating method. *Ceram Int* 35(8):3407–3410
- Du N, Pritzker M (2003) Investigation of electroless plating of Ni-W-P alloy films. *J Appl Electrochem* 33(11):1001–1009
- Ehteram A, Aish H (2008) Corrosion behavior of mild steel in hydrochloric acid solutions. *Int J Electrochem Sci* 3:806–818
- Equbal A, Dixit NK, Sood AK (2013) Electroless plating on plastic. *Int J Sci Eng Res* 8(4):12–18
- Gao W, Cao D, Jin Y, Zhou X, Cheng G, Wang Y (2018) Microstructure and properties of Cu-Sn-Zn- $TiO_2$  nano-composite coatings on mild steel. *Surf Coat Technol* 350:801–806
- Guo D, Zhang M, Jin Z, Kang R (2006) Pulse plating of copper-ZrB<sub>2</sub> composite coatings. *J Mater Sci Technol* 22(4):514–518
- House K, Sernetz F, Dymock D, Sandy JR, Ireland AJ (2008) Corrosion of orthodontic appliances—should we care? *Am J Orthod Dentofac Orthop* 133(4):584–592
- Inoue R, Arai Y, Kubota Y, Kogo Y, Goto K (2018) Oxidation of ZrB<sub>2</sub> and its composites: a review. *J Mater Sci* 53(21):14885–14906
- Jackson M, Deocampo D, Marra F, Scheetz B (2010) Mid-Pleistocene pozzolanic volcanic ash in ancient Roman concretes. *Geoarchaeology* 25(1):36–74
- Jirarungsatien C, Prateepasen A (2010) Pitting and uniform corrosion source recognition using acoustic emission parameters. *Corros Sci* 52(1):187–197
- Kallappa D, Venkatarangaiah VT (2018) Synthesis of CeO<sub>2</sub> doped ZnO nanoparticles and their application in Zn-composite coating on mild steel. *Arab J Chem* 3:45–60
- Krishnan KH, John S, Srinivasan KN, Praveen J, Ganesan M, Kavimani PM (2006) An overall aspect of electroless Ni-P depositions—a review article. *Metall Mater Trans A* 37(6):1917–1926
- Balaraju JN, SankaraNarayanan TSN, Seshadri SK (2003) Electroless Ni-P composite coatings. *J Appl Electrochem* 33(9):807–816
- Agarwala RC, Agarwala V (2003) Electroless alloy/composite coatings: a review. *Sadhana* 28:475–493
- Kumar S, Pande S, Verma P (2015) Factor effecting electro-deposition process. *Int J Curr Eng Technol* 5(2):700–703
- Laudisio G, Seipel B, Ruffini A, Nickel KG (2005) Corrosion behavior of  $Si_3N_4$ -TiN composite in sulphuric acid. *Corros Sci* 47(7):1666–1677
- Li B, Li D, Xia W, Zhang W (2018) Synthesis and characterization of a novel Zn-Ni and Zn-Ni/ $Si_3N_4$  composite coating by pulse electrodeposition. *Appl Surf Sci* 458:665–677
- Constantin I (2014) Microstructural characterization and corrosion behavior of electroless Ni-Zn-P Thin Films. *J Metall* 214:1–6
- Oriňáková R, Turoňová A, Kladeková D, Gálová M, Smith RM (2006) Recent developments in the electrodeposition of nickel and some nickel-based alloys. *J Appl Electrochem* 36(9):957–972
- Pang JN, Jiang SW, Lin H, Wang ZQ (2016) Significance of sensitization process in electroless deposition of Ni on nanosized  $Al_2O_3$  powders. *Ceram Int* 42(3):4491–4497
- Popescu AM, Soare V, Burada M, Mitriță D, Constantin I, Bădiliță V, Minculescu F, Cotrut C, Neacsu EI, Donath C, Constantin V (2018) Electrochemical behaviour of ternary Ni-Zn-P thin films deposition on steel substrate. *Indian J ChemTech* 25:572–577
- Popoola API, Fayomi OSI (2016) Effect of some process variables on zinc coated low carbon steel substrates. *Sci Res Essays* 6(20):4264–4272
- Zarras P, Stenger-Smith JD (2014) Corrosion processes and strategies for prevention: an introduction. *Handb Smart Coat Mater Prot* 64:3–28
- Ahmad YH, Mohamed AMA (2014) Electrodeposition of nano-structured nickel-ceramic composite coatings: a review. *Int J Electrochem Sci* 9(4):1942–1963
- Akande IG, Oluwole OO, Fayomi OSI (2018) Optimizing the defensive characteristics of mild steel via the electrodeposition of Zn- $Si_3N_4$  reinforcing particles. *Def Technol* 14:1–7

**Publisher's Note** Springer Nature remains neutral with regard to jurisdictional claims in published maps and institutional affiliations.